CrossMark

Long-term stability of metal-supported solid oxide fuel cells employing infiltrated electrodes

Yucun Zhou, Ting Chen, Junliang Li, Chun Yuan, Xianshuang Xin, Guoyi Chen, Guoshuan Miao, Weiting Zhan, Zhongliang Zhan, Shaorong Wang*

CAS Key Laboratory of Materials for Energy Conversion, Shanghai Institute of Ceramics, Chinese Academy of Sciences (SICCAS), 1295 Ding-xi Road, Shanghai 200050, China

HIGHLIGHTS

- Both temperatures and current densities affect the cell stability.
- The degradation was mainly caused by the morphological change of the anode.
- A degradation rate of 1.3% kh^{-1} was found during the 1500 h test at 650 °C.

ARTICLE INFO

ABSTRACT

Here, stability of the metal-supported solid oxide fuel cell (MS-SOFC) with $Ni-Ce_{0.8}Sm_{0.2}O_{2-\delta}$ (SDC) infiltrated 430L anode and $La_{0.6}Sr_{0.4}Fe_{0.9}Sc_{0.1}O_{3-\delta}$ (LSFSc) infiltrated scandia-stabilized zirconia (SSZ) cathode is evaluated. It is found that the degradation rate defined as the voltage loss during a fixed period is faster at higher operation temperatures and larger current densities. Scanning electron microscopy (SEM) and energy dispersive X-ray spectra (EDS) analysis indicate that the degradation is mainly caused by the morphological change of the anode while metal element diffusion between Ni catalyst and 430L substrate contributes little. A 1500 h durability test measured at 650 °C and 0.9 A cm^{-2} shows a degradation rate of 1.3% kh^{-1} and the voltage decrease is mainly found in the initial 500 h.

1. Introduction

Metal-supported solid oxide fuel cells (MS-SOFCs) using a porous alloy e.g., ferritic stainless steel as the supporting component have regained wide interest due to the advantages like lower materials cost, improved mechanical strength and enhanced tolerance to redox cycles over the traditional anode- or electrolyte-supported SOFCs [1]. Considerable progress both in fundamental and applied aspects in MS-SOFCs has been obtained in recent years. For example, micro combined heat and power (mCHP) unit based on the MS-SOFC has been demonstrated by Ceres Power [2], a plasma sprayed MS-SOFC stack delivered a power of 606 W at 42.4% fuel utilization has been put forward in the Institute of Nuclear Energy Research in Taiwan [3], the potential of MS-SOFC for mobile applications has also been demonstrated in Plansee [4].

However, before the commercial deployment of the MS-SOFC, several critical issues should be solved. For the anode, oxidation of the porous metal substrate in the humidified hydrogen atmosphere is a problem which would increase the anode area specific resistance (ASR) due to the formation of oxide scales and the metal/oxide scale interfaces [5]. The linear increase in oxide scale growth as the porosity of the metal substrate increased has also been reported [6]. Another critical issue is the metal element diffusion between the Ni based anode and the Fe–Cr based substrate, which will inhibit the electrochemical activity of the anode and change the oxidation behavior and the coefficient of thermal expansion (CTE) of the substrate [7]. As reported, Cr and Fe were diffused to a depth of approximately 50 μm from the STS 430 containing layer to the anode during the operation at 800 °C for about 800 h [8]. Additionally, Ni coarsening is also a problem, especially for the

infiltrated anode. For example, a rapid power degradation of a MS-SOFC with infiltrated Ni catalysts was found at 700 °C [9]. Our previous work also demonstrated a degradation rate of approximately 11%/100 h at 650 °C for a MS-SOFC and the degradation mainly resulted from rapid coarsening of the infiltrated nano-scale Ni catalysts [10]. Despite the issues coming from the cell anode, the poor chemical compatibility and thermal expansion compatibility between the cathodes and the traditional electrolyte materials also affect the cell stability [8,11]. For the oxidation behavior of the metal support at high temperature in air, it is difficult to sinter the traditional cathode materials such as $La_{1-x}Sr_xMnO_{3-\delta}$ (LSM) which needs to be sintered in air at 1000–1200 °C. Sintering the cathodes in-situ at the temperature of 800–850 °C is an effective way to solve the problem while cathode materials like $(La_{0.6}Sr_{0.4})_{0.99}CoO_3$ (LSC) and $La_{0.58}Sr_{0.4}Co_{0.2}Fe_{0.8}O_3$ (LSCF) with higher sintering capabilities are needed [12]. However, one of the drawbacks of these cathodes is the poor chemical compatibility with the zirconia-based electrolytes. For example, the maximum power density (MPD) of a MS-SOFC with $Ba_{0.5}Sr_{0.5}Co_{0.8}Fe_{0.2}O_{3-\delta}$ (BSCF) cathode decreased from 0.81 to 0.63 W cm^{-2} after operating at 850 °C for 50 h [11]. The interaction between BSCF and yttria-stabilized zirconia (YSZ) which promotes $SrZrO_3$ and $BaZrO_3$ secondary phases was responsible for the degradation. Another issue of these in-situ sintered cathodes is the thermal expansion compatibility with the electrolyte materials. A MS-SOFC with $Sm_{0.5}Sr_{0.5}CoO_3$ (SSC)–$Ce_{0.8}Sm_{0.2}O_{2-\delta}$ (SDC) cathode showed rapid performance decrease after first two thermal cycles and the degradation was mainly due to the CTE mismatch between the SDC electrolyte layer and the SSC–SDC composite cathode [13]. Thermal expansion mismatch was also found to be one of the degradation mechanisms of the MS-SOFC employing NiO-SDC anode, SDC electrolyte and SSC–SDC composite cathode [14].

Preparing the electrodes by the infiltration method can circumvent the above issues while coarsening of the infiltrated nano particles is another problem [9,10,15–17]. In our previous work, a MS-SOFC comprising of Ni-SDC infiltrated 430L (16–18 wt% Cr-based ferritic stainless steel alloy) anode, YSZ electrolyte and $La_{0.6}Sr_{0.4}Fe_{0.9}Sc_{0.1}O_{3-\delta}$ (LSFSc) infiltrated YSZ cathode was successfully fabricated [16]. Promising performance of such cell was obtained at the temperature range of 650–800 °C and short-term stability was demonstrated at 600 °C. In this study, long-term stability of this kind of MS-SOFC was further studied and effects of temperature and current density on the cell stability were evaluated.

2. Experimental

The cell scaffold of porous 430L support/dense scandia-stabilized zirconia (SSZ) electrolyte/porous SSZ layer was produced by the tape casting, laminating and co-firing method [16]. Commercially available 430L stainless steel powder (−400 mesh, Jing-yuan Powder Material Co., Ltd, China) and SSZ powder $((ZrO_2)_{0.89}(Sc_2O_3)_{0.1}(CeO_2)_{0.01}$, Daiichi kigenso kagaku kogyo Co., Ltd, Japan) were used as the starting materials. The slurry for tape casting was based on ethanol solvent, containing acrylic resin dispersant, polyvinyl butyral binder, dibutyl phthalate plasticizer and other organic additives, in addition to powder. After drying, green sheets of 430L support, SSZ electrolyte and SSZ cathode backbone were laminated and co-sintered in a reducing atmosphere of 5% H_2/95% N_2 at 1320 °C for 4 h. After the cell scaffold preparation, $Ni(NO_3)_2$, $Sm(NO_3)_3$ and $Ce(NO_3)_3$ aqueous solution in stoichiometric ratios (the mass ration of SDC:Ni = 8:2) was introduced into the porous 430L support by the infiltration method. After that, the LSFSc cathode catalyst was introduced into the porous cathode backbone by infiltration of an aqueous solution

containing stoichiometric amounts of $La(NO_3)_3$, $Sr(NO_3)_2$, $Fe(NO_3)_3$ and $Sc(NO_3)_3$, where citric acid was also added at a 1:1 molar ratio to metal ions (99% pure, Sinopharm Chemical Reagent Co., Ltd.). After drying, heat treatment was conducted at 850 °C in 5% H_2 – 95% N_2 for 2 h to convert these salts into metal oxides. The reducing atmosphere was applied to protect the 430L substrate from excessive oxidation and the low sintering temperature was chosen to avoid the possible reaction between the cathode and the electrolyte. The infiltration/heat treatment cycle was repeated to increase the amounts of the infiltrated catalysts. A single infiltration/heat treating cycle yielded a loading of ≈5 wt% for the cathode and ≈3 wt% for the anode. 30 wt% catalyst loading for the cathode and 10 wt% catalyst loading for the anode were applied as we optimized previously [18,19].

For electrochemical measurements, the single cells were sealed onto alumina tubes using the silver paste (DAD-87, Shanghai Research Institute of Synthetic Resins) and silver current collectors were applied to both electrodes for electrical connections. Current–voltage (I–V) curves and electrochemical impedance spectra (EIS) were obtained by using an IM6 Electrochemical Workstation (ZAHNER, Germany) over the temperatures range of 600–800 °C with the cathode exposed to air and the anode to humidified (3% H_2O) hydrogen, both at the flow rate of 100 mL min^{-1}. I–V curves were measured in the galvanostatic mode and EIS were collected under open circuit conditions with a 20 mV AC amplitude over the frequency range of 100 mHz–0.2 MHz. The area specific ohmic resistance (Ro) corresponds to the high-frequency real-axis intercept and the area specific polarization resistance (Rp) was determined by the difference of the low- and high-frequency intercepts of the impedance spectra with the real axis. For long-term stability test, the cell was operated at 600, 650 and 700 °C at different current densities with humidified (3% H_2O) hydrogen and air. Active area of the single cell was 0.35 cm^2.

Microstructures of the fuel cell were examined by scanning electron microscopy (SEM) using Hitachi S-4800-II and SU-8220 microscopes. Element distributions were analyzed using a JEOL JXA-8100 electron probe microanalyzer (EPMA).

3. Results and discussion

Photograph of the MS-SOFC backbone (porous 430L support/dense SSZ electrolyte/porous SSZ layer) after sintering at 1320 °C in 5% H_2/95% N_2 is shown in Fig. 1(a). The cell was flat with a diameter of 1.5 cm. Fig. 1(b) shows the cross-sectional SEM micrograph of SOFC containing a porous Ni-SDC infiltrated 430L anode (≈260 μm), a dense SSZ electrolyte (≈17 μm) and a porous LSFSc infiltrated SSZ cathode (≈30 μm). In this study, the Ni-SDC infiltrated 430L both acts as the cell support and the cell anode. The electrolyte was fully dense without obvious pores. Fig. 1(c) and (d) show a higher-magnification SEM micrograph of the Ni-SDC infiltrated 430L anode (10 wt% loading) and LSFSc infiltrated SSZ cathode (30 wt% loading), respectively. Coatings consist of nano and porous particles were well connected with the electrode backbones.

Electrochemical characteristics of the single MS-SOFC operating on humidified hydrogen fuel and air oxidant at 600–800 °C are shown in Fig. 2. Fig. 2(a) shows that the maximum power densities (MPDs) measured were 0.30, 0.53, 0.78, 1.00 and 1.22 W cm^{-2} at 600, 650, 700, 750 and 800 °C, respectively. Nyquist plots of the impedance data as obtained at open circuit voltage (OCV) for the present MS-SOFC is shown in Fig. 2(b). The pure ohmic losses correspond to the high-frequency real-axis intercepts and the polarization resistances are taken by subtracting the ohmic resistances from the total resistances (low-frequency intercepts at real-axis). The pure ohmic resistance were 0.10, 0.13, 0.17, 0.24
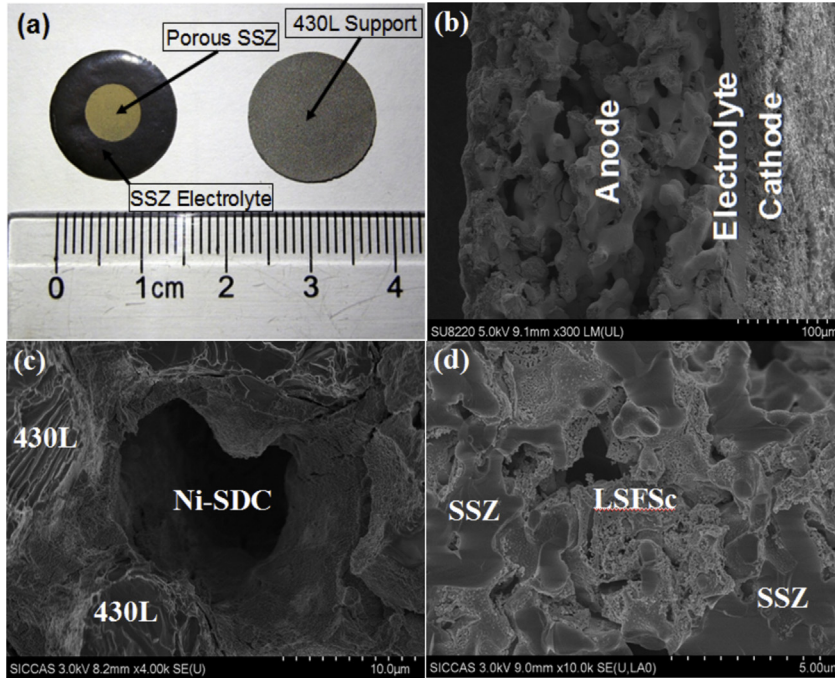
Fig. 1. (a) Photograph of the button cell (before infiltrating) viewed from the electrolyte side (left) and the 430L support side (right), Cross-sectional scanning electron microscope (SEM) images of the MS-SOFC: (b) The single cell, (c) The Ni-SDC infiltrated 430L anode and (d) The LSFSc infiltrated SSZ cathode.

and 0.37 Ω cm^2 and the polarization resistance were 0.16, 0.20, 0.24, 0.35 and 0.43 Ω cm^2 at 800, 750, 700, 650 and 600 °C, respectively. Compared to the ohmic resistance, the polarization resistance plays a more dominate role in the cell performance.
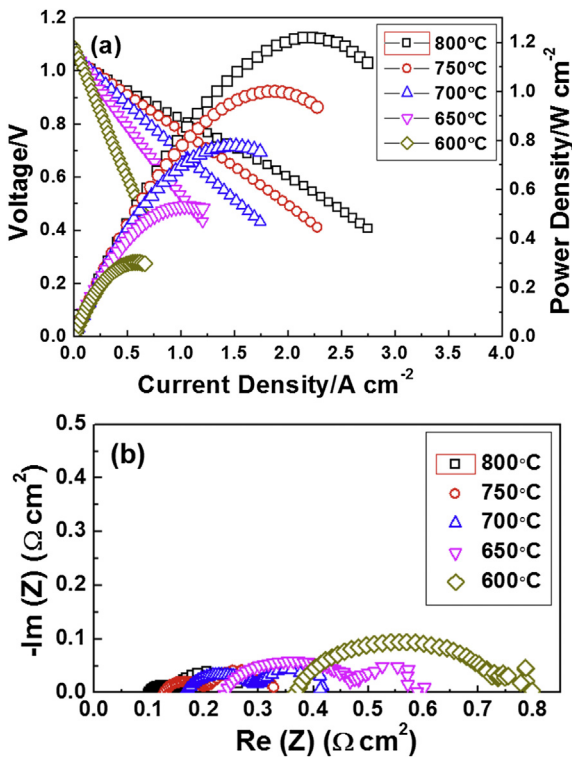

Fig. 2. Electrochemical characteristics of the MS-SOFC measured at 600–800 °C: (a) Voltage and power density versus current density and (b) Impedance spectra at open circuits.

Short-term stabilities of the single MS-SOFC measured at 700–600 °C are shown in Fig. 3. Rapid voltage decrease (from 0.804 to 0.645 V) was found when measured at 700 °C with a current density of 0.86 A cm^{-2} (Fig. 3(a)). Note that reducing the operation temperature and current density exhibit a more stable performance. As shown in Fig. 3(b), a slight decrease of voltage from 0.70 to 0.694 V was observed during the 357 h measurement at 650 °C and 0.57 A cm^{-2}. No degradation was found when further reducing the operation temperature to 600 °C and current density to 0.4 A cm^{-2} (Fig. 3(c)).

I−V−P characteristics of the MS-SOFC measured after the 0, 80 and 175 h operation at 700 °C is shown in Fig. 4(a). A decrease of MPD from 0.72 to 0.62 W cm^{-2} was found during the 80 h operation. Continued operation caused gradual degradation, e.g., a MPD of 0.55 W cm^{-2} was obtained when measured at 175 h. Nyquist plots of the impedance data obtained before and after the stability test are shown in Fig. 4(b). The increase of total resistance from 0.34 to 0.51 Ω cm^2 should be the reason to the cell performance degradation. During the 175 h stability test, the Ro increased from 0.10 to 0.15 Ω cm^2 while the Rp changed from 0.24 to 0.36 Ω cm^2. As reported, the conductivity of the porous 430L could remain 15 S cm^{-1} after oxidating in air at 700 °C for 178 h. Take the fact that the oxidation in air is more rapid than in humidified hydrogen, the increase in ohmic resistance caused by the formation of a corrosion scale is negligible in this study [20]. It seems that the ohmic resistance increase is more likely caused by the reduced adhesion between the 430L support and the electrolyte. This adhesion problem has been identified by the post mortem SEM of the MS-SOFC. From Bode plots of the EIS collected at OCV before and after the stability test (Fig. 4(c)), it is observed that the Rp change was characterized by the increased impedance at intermediate frequencies between 100 Hz and 10 kHz. As reported, for the Ni:CGO infiltrated cermet anode, the high frequency impedance arc was attributed to the oxide ion charge transfer resistance between the electrolyte and the infiltrated anode (summit frequency around 500 kHz), the intermediate frequency arc (summit frequency
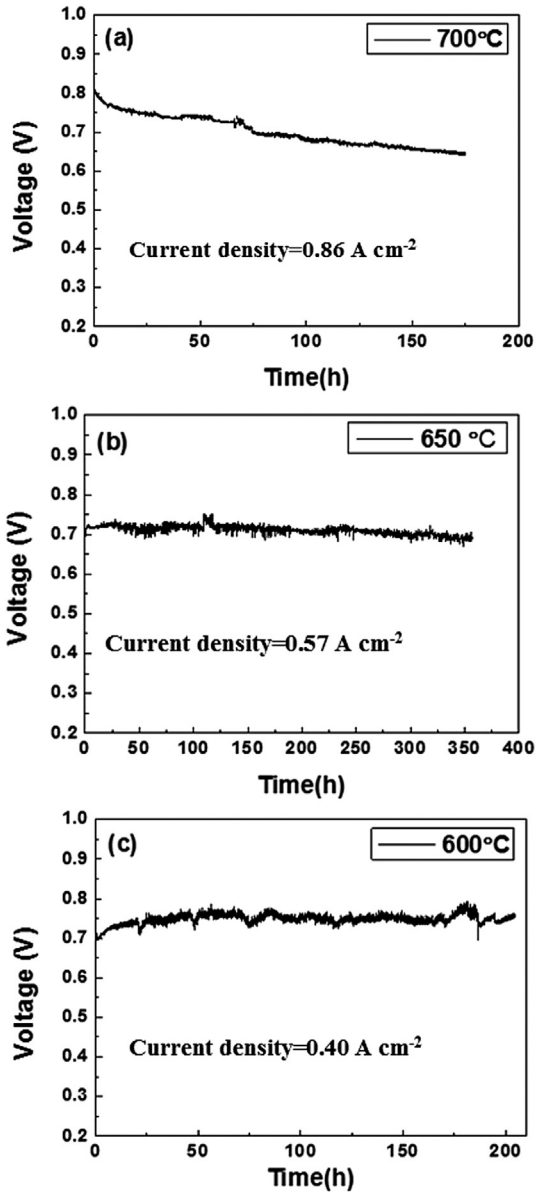
Fig. 3. Short-term stability of the single MS-SOFC measured at: (a) 700 °C, (b) 650 °C and 600 °C.
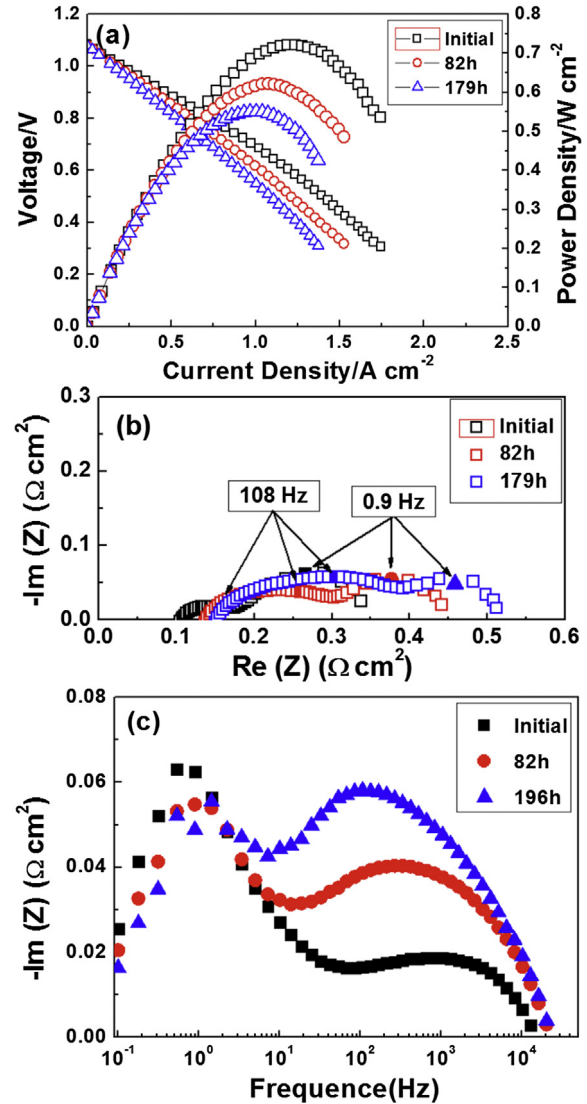

Fig. 4. Electrochemical characteristics of the MS-SOFC before and after the stability test measured at 700 °C: (a) Voltage and power density versus current density, (b) Nyquist plots of the impedance spectra and (c) Bode plots of the impedance spectra.

around 300 Hz) was ascribed the electrochemistry of the electrode reaction, while the low frequency arc (summit frequency around 4 Hz) was shown to be related to the gas composition [21,22]. Similar conclusion has also been found in the $La_{0.6}Sr_{0.4}CoO_{3-\delta}$ infiltrated $Ce_{0.9}Gd_{0.1}O_{1.95}$ cathode [23]. Since the infiltrated particles are easy to be coarsened, we surmise that the micrographs change of the cell electrodes which would decrease the active surface area should be the main reason to the increase of the polarization resistance [9,19].

To verify the surmise above, SEM micrographs of the Ni-SDC infiltrated 430L anodes and LSFSc infiltrated SSZ cathodes before and after the durability tests were examined. As shown in Fig. 5(a0)–(a3), coarsening of the particles and cracking of the infiltrated coatings were clearly observed for the anodes measured after the stability tests carried out at temperature range of 600−700 °C. In contrast, no obvious changes in the morphologies of the LSFSc infiltrated SSZ cathodes were observed before and after the stability tests (Fig. 5(b0)–(b3)). This is consistent with our

previous report which showed that no pronounced changes both in LSFSc particle size and morphology were observed after the 400 h durability test measured at 650 °C [10]. Based on the SEM results shown in Fig. 5, we can conclude that morphological change of the infiltrated Ni-SDC coating reducing the TPB length should be the main reason to the cell performance degradation. Previous work showed that higher operation temperatures and higher current densities could accelerate the coarsening of the electrodes [24−27]. That should be the reason why the morphological change was particularly serious for the anode tested at 700 °C and 0.86 A cm^{-2} (Fig. 5(a1)).

It is reported that the metal element diffusion between the Ni based anode and the Fe−Cr based substrate could be a key factor for rapid cell degradation [8,28]. In order to identify whether interdiffusions of Fe, Ni and Cr occurred in this study, energy dispersive X-ray spectroscopy (EDS) spectrums of the 430L backbones before and after the stability tests were measured (Fig. 6). All of the samples reflected the compositions of Fe−Cr and no Ni element was detected. It suggests that the metal element diffusion issue may not be the problem here.
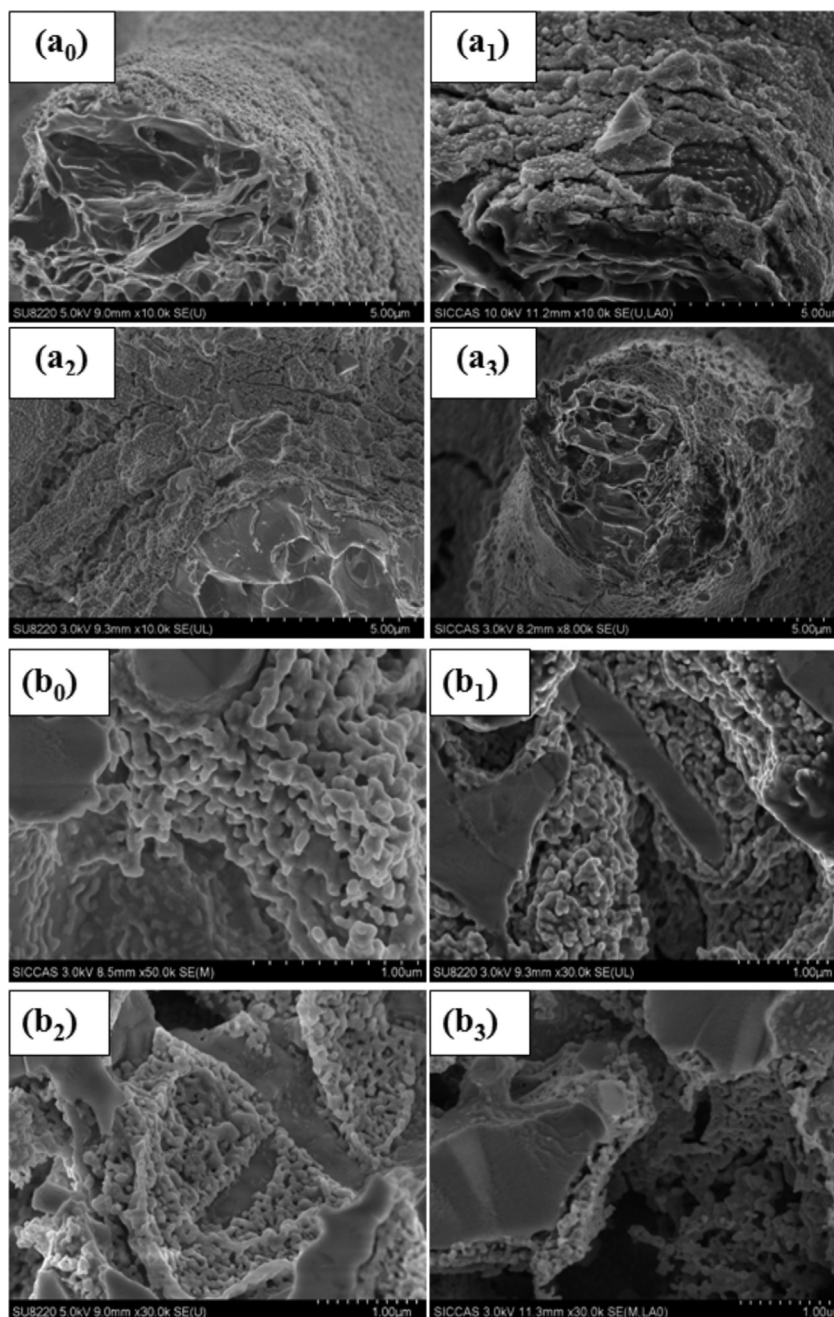
Fig. 5. Microstructures of the Ni-SDC infiltrated 430L anode: (a_0) Before the stability test, and after the stability test measured at (a_1) 700 °C, (a_2) 650 °C, (a_3) 600 °C, Microstructures of the LSFSc infiltrated SSZ cathode: (b_0) Before the stability test, and after the stability test measured at (b_1) 700 °C, (b_2) 650 °C, (b_3) 600 °C.

Since both the temperature and the current load are varied in Fig. 3, it is hard to identify the impact of current density and temperature on degradation independently. Stabilities of the MS-SOFC measured at varied current densities and temperatures were further studied and shown in Fig. 7. To evaluate the impact of current density on degradation, we kept the temperature constant. As shown in Fig. 7, the degradation rate was 9.23% (from 0.802 to 0.728 V) when measured at 700 °C and 0.86 A cm^{-2}, while a much higher degradation rate of 15.57% (from 0.501 to 0.423 V) was found when the fuel cell operated under a higher current density of 1.23 A cm^{-2}. Furthermore, to evaluate the impact of temperature on degradation, the applied current densities were kept similar (0.86 A cm^{-2} at 700 °C and 0.90 A cm^{-2} at 650 °C). It is found that

the degradation rate was 9.23% (from 0.802 to 0.728 V) and 2.61% (from 0.537 to 0.523 V) when measured at 700 °C and 650 °C, respectively. In conclusion, both the current density and temperature have great impact on the stability of the MS-SOFC and larger current density and higher temperature would cause more significant degradation.

Long-term stability of the single cell operated at 650 °C under a high current density of 0.9 A cm^{-2} is shown in Fig. 8. Voltage decrease was found in the initial 500 h while no obvious change was found during the subsequent 1000 h measurement. It is consistent with the durability test of the Ni-SDC infiltrated 430L anode, which showed that the polarization resistance of the anode increases from 0.12 to 0.3 Ω cm^2 during the initial 500 h while no

(a)

Element	App Conc.	Intensity Corrn.	Weight%	Weight% Sigma	Atomic%
Si K	0.51	0.6800	1.01	0.16	1.96
Cr K	15.95	1.1554	18.75	0.41	19.67
Fe K	57.10	0.9664	80.24	0.43	78.37
Totals			100.00		

(b)

Element	App Conc.	Intensity Corrn.	Weight%	Weight% Sigma	Atomic%
Si K	0.36	0.6807	0.74	0.13	1.44
Cr K	16.65	1.1497	20.32	0.43	21.35
Fe K	54.25	0.9643	78.94	0.44	77.21
Totals			100.00		

(c)

Element	App Conc.	Intensity Corrn.	Weight%	Weight% Sigma	Atomic%
Si K	0.52	0.6814	0.96	0.16	1.87
Cr K	18.47	1.1485	20.33	0.38	21.31
Fe K	60.02	0.9639	78.71	0.41	76.82
Totals			100.00		

(d)

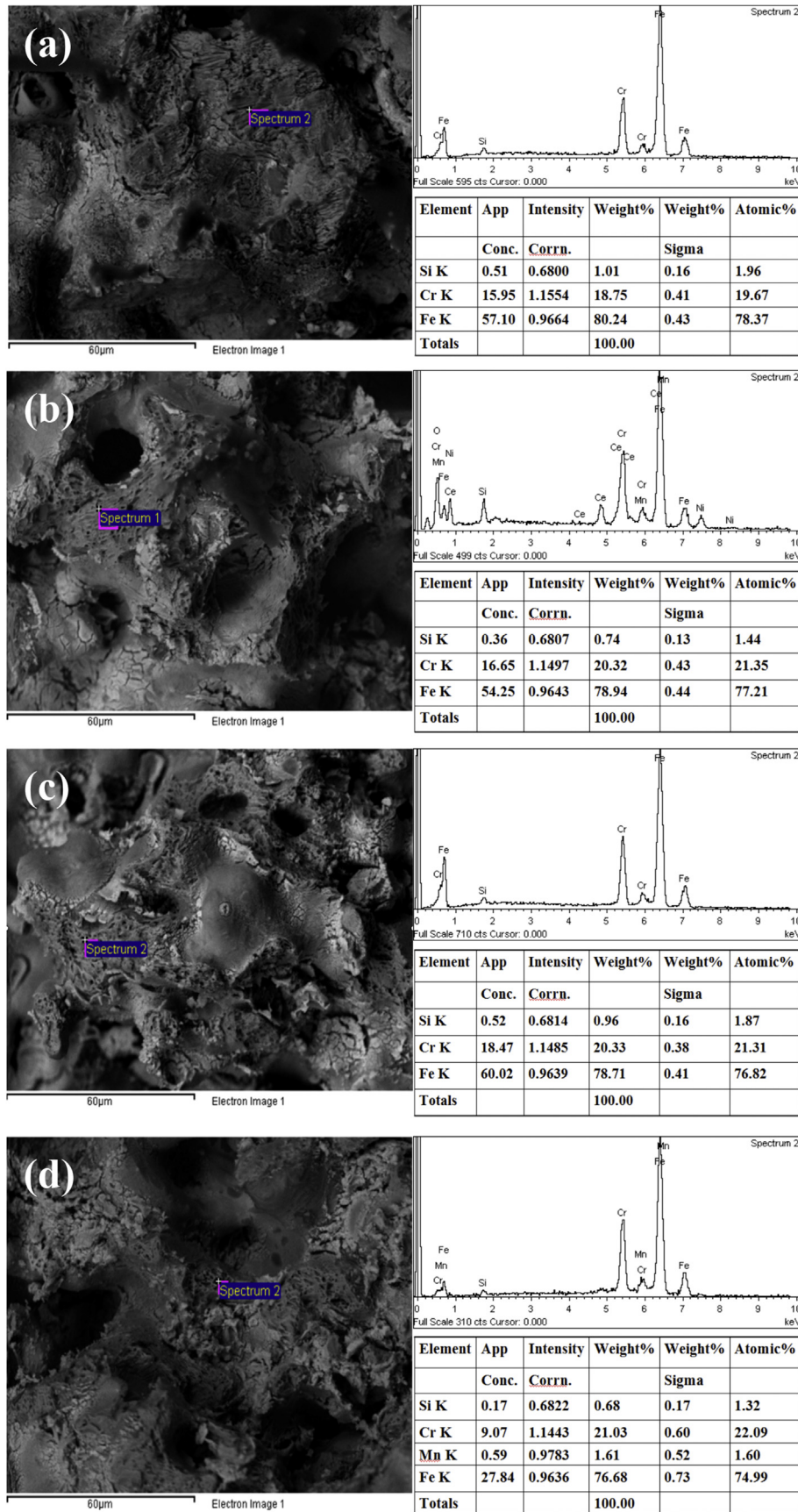| Element	App Conc.	Intensity Corrn.	Weight%	Weight% Sigma	Atomic%
Si K	0.17	0.6822	0.68	0.17	1.32
Cr K	9.07	1.1443	21.03	0.60	22.09
Mn K	0.59	0.9783	1.61	0.52	1.60
Fe K	27.84	0.9636	76.68	0.73	74.99
Totals			100.00		

Fig. 6. Energy-dispersive X-ray spectroscopy (EDS) spectrums of the 430L backbone: (a) Before the stability test, and after the stability test measured at (b) 700 °C, (c) 650 °C, (d) 600 °C.
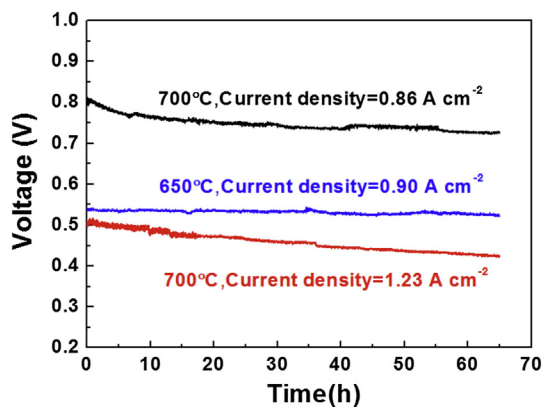
Fig. 7. Stabilities of the MS-SOFC measured at varied current densities and temperatures.
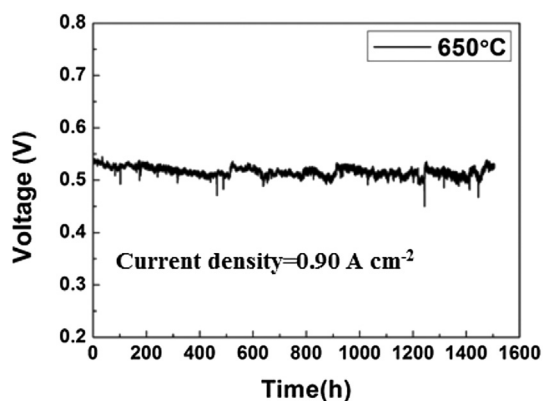

Fig. 8. Long-term stability of the single MS-SOFC measured at 650 °C.

degradation is found during the subsequent measurement at 650 °C [19]. This result further confirms our conclusion that the cell degradation was caused by the anode. As shown in Fig. 8, during the 1500 h measurement, a degradation rate of 1.3% kh^{-1} in cell voltage was found. Another MS-SOFC with a FeCr alloy support, CGO-Ni infiltrated cermet anode, ScYSZ electrolyte and LSCF cathode exhibited a more stable performance, i.e., 0.9% kh^{-1} at 650 °C [17]. The differences in cell durability may be caused by the different current densities, e.g., current load of 0.9 A cm^{-2} was applied here while it was only 0.25 A cm^{-2} in that report. Additionally, diverse materials and cell structures could also be the reasons. Note that silver was used as the sealant and current collector in this study. As reported, migration/deposition of Ag to the TPB would happen during the operating process, which can potentially catalyze the oxygen reduction reaction [29,30]. Thus, the real degradation rate may be different (probably higher) than we measured. In order to eliminate the influence of Ag, stabilities of the fuel cell should be further tested using the ceramic sealant and Au current collector.

4. Conclusions

A MS-SOFC comprising a Ni-SDC infiltrated 430L anode, SSZ electrolyte and LSFSc infiltrated SSZ cathode was fabricated by the tape casting, co-firing and infiltration method. Durability tests of the single cell shown that a more rapid degradation was found when operated at a higher temperature and a larger current density, e.g., the degradation rate was 2.61% when measured at

0.90 A cm^{-2} and 650 °C, a higher degradation rate of 9.23% was observed at 0.86 A cm^{-2} and 700 °C, a much higher degradation rate of 15.57% was found when the current density improved to 1.23 A cm^{-2} (700 °C). SEM and EDS examinations shown that the morphological change of the anode should be the main reason to the cell degradation while metal element diffusion between Ni catalyst and 430L substrate may not be the problem. A 1500 h durability test measured at 650 °C and 0.9 A cm^{-2} showed that the degradation rate of the single cell was 1.3% kh^{-1} and the voltage decrease was mainly found in the initial 500 h.

References

[1] M.C. Tucker, J. Power Sources 195 (2010) 4570–4582.
[2] R.T. Leah, A. Bone, A. Selcuk, D. Corcoran, M. Lankin, Z. Dehaney-Steven, M. Selby, P. Whalen, ECS Trans. 35 (2011) 351–367.
[3] C.-S. Hwang, C.-H. Tsai, C.-L. Chang, C.-M. Chuang, Z.-Y.C. Shie, S.-W. Cheng, S.-H. Wu, Thin Solid Films 570 (Part B) (2014) 183–188.
[4] T. Franco, M. Haydn, A. Weber, W. Schafbauer, L. Blum, U. Packbier, D. Roehrens, N.H. Menzler, J. Rechberger, A. Venskutonis, L.S. Sigl, H.P. Buchkremer, ECS Trans. 57 (2013) 471–480.
[5] N. Shaigan, W. Qu, D.G. Ivey, W. Chen, J. Power Sources 195 (2010) 1529–1542.
[6] E. Sarasketa-Zabala, L. Otaegi, L.M. Rodriguez-Martinez, M.A. Alvarez, N. Burgos, F. Castro, I. Villarreal, Solid State Ionics 222 (2012) 16–22.
[7] T. Franco, K. Schibinger, Z. Ilhan, G. Schiller, A. Venskutonis, ECS Trans. 7 (2007) 771–780.
[8] J.H. Choi, T. Lee, M. Choi, Y.-S. Yoo, S.-W. Baek, J. Bae, Int. J. Hydrogen Energy 35 (2010) 4285–4291.
[9] M.C. Tucker, G.Y. Lau, C.P. Jacobson, L.C. DeJonghe, S.J. Visco, J. Power Sources 175 (2008) 447–451.
[10] Y. Zhou, X. Xin, J. Li, X. Ye, C. Xia, S. Wang, Z. Zhan, Int. J. Hydrogen Energy 39 (2014) 2279–2285.
[11] Y.-M. Kim, P. Kim-Lohsoontorn, J. Bae, J. Power Sources 195 (2010) 6420–6427.
[12] J. Nielsen, P. Hjalmarsson, M.H. Hansen, P. Blennow, J. Power Sources 245 (2014) 418–428.
[13] Z. Wang, J.O. Berghaus, S. Yick, C. Deces-Petit, W. Qu, R. Hui, R. Maric, D. Ghosh, J. Power Sources 176 (2008) 90–95.
[14] Q.-A. Huang, B. Wang, W. Qu, R. Hui, J. Power Sources 191 (2009) 297–303.
[15] M.C. Tucker, G.Y. Lau, C.P. Jacobson, L.C. DeJonghe, S.J. Visco, J. Power Sources 171 (2007) 477–482.
[16] Y. Zhou, X. Ye, J. Li, Z. Zhan, S. Wang, J. Electrochem. Soc. 161 (2014) F332–F336.
[17] T. Klemenso, J. Nielsen, P. Blennow, A.H. Persson, T. Stegk, B.H. Christensen, S. Sonderby, J. Power Sources 196 (2011) 9459–9466.
[18] Y. Zhou, X. Meng, X. Ye, J. Li, S. Wang, Z. Zhan, J. Power Sources 247 (2014) 556–561.
[19] Y. Zhou, C. Yuan, T. Chen, X. Meng, X. Ye, J. Li, S. Wang, Z. Zhan, J. Power Sources 267 (2014) 117–122.
[20] S. Molin, B. Kusz, M. Gazda, P. Jasinski, J. Power Sources 181 (2008) 31–37.
[21] P. Blennow, J. Hjelm, T. Klemenso, A.H. Persson, S. Ramousse, M. Mogensen, Fuel Cells 11 (2011) 661–668.
[22] J. Nielsen, T. Klemenso, P. Blennow, J. Power Sources 219 (2012) 305–316.
[23] A. Samson, M. Søgaard, R. Knibbe, N. Bonanos, J. Electrochem. Soc. 158 (2011) B650–B659.
[24] X. Meng, D. Han, H. Wu, J. Li, Z. Zhan, J. Power Sources 246 (2014) 906–911.
[25] Y. Zhou, D. Han, C. Yuan, M. Liu, T. Chen, S. Wang, Z. Zhan, Electrochim. Acta 149 (2014) 231–236.
[26] T. Komatsu, Y. Yoshida, K. Watanabe, R. Chiba, H. Taguchi, H. Orui, H. Arai, J. Power Sources 195 (2010) 5601–5605.
[27] T. Hatae, Y. Matsuzaki, S. Yamashita, Y. Yamazaki, Solid State Ionics 180 (2009) 1305–1310.
[28] M. Brandner, M. Bram, J. Froitzheim, H.P. Buchkremer, D. Stoever, Solid State Ionics 179 (2008) 1501–1504.
[29] J. Nielsen, T. Jacobsen, Solid State Ionics 178 (2008) 1769–1776.
[30] S.P. Simner, M.D. Anderson, L.R. Pederson, J.W. Stevenson, J. Electrochem. Soc. 152 (2005) A1851–A1859.